Highly squeezed states in ring resonators: Beyond the undepleted-pump approximation

Colin Vendromin [1,*] Yan Liu,[2] Zhenshan Yang,[2] and J. E. Sipe[1]

[1]*Department of Physics, University of Toronto, 60 St. George Street, Toronto, Ontario, Canada M5S 1A7*

[2]*School of Physics Science and Information Technology, Shandong Key Laboratory of Optical Communication Science and Technology,
Liaocheng University, Liaocheng 252059, China*

We present a multimode theory of squeezed-state generation in resonant systems valid for arbitrary pump power and including pump depletion. The Hamiltonian is written in terms of asymptotic-in and -out fields from scattering theory, capable of describing a general interaction. As an example we consider the lossy generation of a highly squeezed state by an effective second-order interaction in a silicon nitride ring resonator point coupled to a waveguide. We calculate the photon number, the Schmidt number, and the second-order correlation function of the generated state in the waveguide. The treatment we present provides a path forward to study the deterministic generation of non-Gaussian states in resonant systems.

I. INTRODUCTION

Continuous-variable (CV) squeezed states of light exhibit an uncertainty below vacuum noise in one quadrature [1], making them an essential resource for implementing CV quantum information processing [2], and with postselection strategies they can be used to create non-Gaussian states of light [3,4], an important resource for quantum computing. Squeezed states are typically generated through nonlinear optical processes such as spontaneous parametric down-conversion (SPDC) and spontaneous four-wave mixing (SFWM), the first relying on the presence of a $\chi^{(2)}$ susceptibility and the second on the $\chi^{(3)}$ susceptibility [5,6]. In the usual treatment of these processes, the pump field or fields are treated classically, with the nonlinear process being considered sufficiently weak that those fields can be treated as undepleted. In this case the resulting squeezed state can be approximately written as [7]

$$|\psi\rangle = \exp\left(\frac{\beta}{2} \int dk_1 k_2 \phi(k_1, k_2) a_{k_1}^\dagger a_{k_2}^\dagger - \text{H.c.}\right)|\text{vac}\rangle, \quad (1)$$

where β is an overall squeezing parameter and $\phi(k_1, k_2)$ is the normalized biphoton wave function that describes the production of pairs of photons, one with wave number k_1 and the other k_2. The ket in Eq. (1) can be obtained by keeping the lowest-order term in the Magnus expansion [8] and treating the pump as classical and undepleted. If the squeezing parameter β is sufficiently weak, then time-ordering corrections that arise in the higher-order terms of the Magnus expansion are expected to be negligible. However, time-ordering effects become important when the amount of squeezing increases [9–11], and the approximate ket in Eq. (1) then becomes a poorer and poorer approximation.

Including time-ordering corrections, the ket can be obtained under the assumption that the pump is classical and undepleted and that the generated light is Gaussian. As a result, the full Gaussian ket can be written generally as a squeezed vacuum state

$$|\psi\rangle = \exp\left(\frac{1}{2} \int dk_1 dk_2 J(k_1, k_2) a_{k_1}^\dagger a_{k_2}^\dagger - \text{H.c.}\right)|\text{vac}\rangle, \quad (2)$$

where the squeezing matrix $J(k_1, k_2)$ can be obtained from the Heisenberg equations of motion [10]. If time-ordering corrections are negligible, this ket reduces to Eq. (1), with the squeezing matrix just being proportional to the biphoton wave function $J(k_1, k_2) \approx \beta\phi(k_1, k_2)$.

However, if the nonlinear process is strong enough that pump depletion needs to be considered, the generated light can be expected to be non-Gaussian due to entanglement between the pump and the generated fields [12,13]. In this case a squeezed vacuum state such as in Eq. (2) does not provide a complete description of the features of the generated light, such as pump depletion. To go beyond the undepleted pump approximation, one strategy that has been employed is to replace the vacuum state in Eq. (2) with a non-Gaussian ket, which starts from the vacuum initially and evolves such that it remains close to the vacuum. This treatment was recently investigated in waveguides [12] and for a single-mode SPDC Hamiltonian [13] and offers a potential route to the deterministic generation of non-Gaussian states of light. In fact, experiments have already demonstrated high conversion efficiencies where the undepleted pump approximation is no longer valid [14,15] and non-Gaussianity may become important.

In this paper we extend such a treatment to resonant systems. As an example we study a ring resonator, a system of interest in its own right due to its resonant enhancement of nonlinear processes and the precise control over the frequencies involved, as well as its integrability on photonic chips [16–18]. We develop a multimode Hamiltonian theory

---

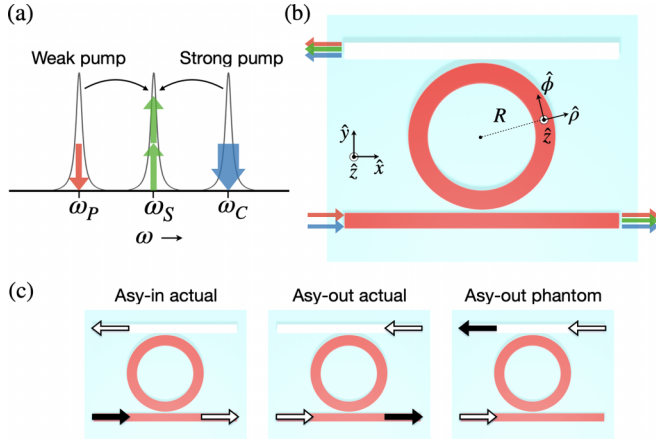*Contact author: colin.vendromin@utoronto.ca

FIG. 1. (a) SFWM with a weak pump at ω_P and a strong pump at ω_C. (b) Schematic of a ring resonator point coupled to an actual waveguide (bottom red) and phantom waveguide (top white). (c) Asymptotic-in field associated with the input channel of the actual waveguide (left) and asymptotic-out fields associated with the output channel of the actual waveguide (center) and phantom waveguide (right) [19,21].

of non-Gaussian state generation in such systems, including scattering loss, by employing the asymptotic-in and -out fields used in scattering theory [19].

We apply the theory to the particular case of generating a highly squeezed state by an effective $\chi^{(2)}$ interaction in a ring resonator [15,20]. For this interaction one relies on the $\chi^{(3)}$ response of the medium, but there is one pump field in a mode C that is a continuous wave (cw) and so strong that it can be treated as classical and undepleted; in the presence of the material $\chi^{(3)}$ this leads to an effective $\chi^{(2)}$ through which a much weaker pump in the mode P can generate two photons in the mode S [see Fig. 1(a)]. There is no issue with phase matching, since the pumps and the generated photons are close in wavelength. The formalism we present can also be applied to a standard $\chi^{(2)}$ interaction as well.

Although the theory we present is capable of studying non-Gaussian states, our focus in this paper is on highly squeezed states that include the effects of pump depletion. The treatment of the non-Gaussian corrections to the squeezed state, the effects of self- and cross-phase modulation, and the excitation of fields in additional ring resonances are beyond the scope of the present work. In the ring resonator and pumping scenario that we study we find that the non-Gaussian corrections to the squeezed state are negligible, justifying our focus on squeezed states. While in this paper we specialize to ring resonator systems, most of the formalism can be applied to other systems as well, such as waveguides.

This paper is organized as follows. In Sec. II we write the system Hamiltonian, including the SFWM interaction in a ring resonator, in terms of the asymptotic-in and -out fields for our system. In Sec. III we introduce the input and output kets that are used to describe the generation of light in the ring resonator system. In Sec. IV we derive the non-Gaussian unitary operator that connects the input ket to the output ket. In Sec. V we show how to obtain the first-order solution for the ket. In Sec. VI we numerically study the generation of a

highly squeezed state by an effective $\chi^{(2)}$ interaction in a ring resonator with loss. In Sec. VII we summarize.

II. THE HAMILTONIAN

Our system of interest is a ring resonator point coupled to an actual waveguide and a phantom waveguide [see Fig. 1(b)], where the phantom waveguide is used to describe scattering losses [21]. We define the input and output channels of the actual waveguide (shown in red) as the parts of that waveguide that are to the left and to the right of the coupling point, respectively; likewise, the input and output channels of the phantom waveguide (shown in white) are the parts of that waveguide that are to the right and to the left of the coupling point, respectively.

As a basis for expanding the electromagnetic field in the full system of waveguides and ring, we employ the asymptotic-in and -out mode fields [19,21]; they are sketched in Fig. 1(c) and are eigenstates of the full linear Hamiltonian of the system. Each asymptotic-in or -out mode field has an amplitude in both waveguides and in the ring. In each diagram, the black arrow corresponds to a freely propagating field that is either incoming (asymptotic-in) or outgoing (asymptotic-out), with its amplitude equal to that of a mode field in an isolated waveguide. The white arrows indicate either outgoing (asymptotic-in) or incoming (asymptotic-out) fields in the other channels, and their amplitudes depend on the coupling parameters between the ring and the waveguides [21]. Asymptotic-in mode fields are also defined for the phantom channel, but they will not appear in our calculations.

The asymptotic-in and -out mode fields can be identified by three parameters. We use a discrete index n to indicate the actual output channel or the phantom output channel, the waveguide wave numbers k, and an index J that identifies the range of wave numbers k in the waveguide that correspond to a range of frequencies near a ring resonance, where $J = P, S, C$. We assume the ring resonances have sufficiently-high-quality factors that the ranges over which k varies for each J can be considered distinct; we leave this implicit in the integrals below.

For the system considered here, the displacement field operator can be written in terms of the asymptotic-in mode fields as [19]

$$\boldsymbol{D}(\boldsymbol{r}) = \sum_{n,J} \int dk \, b_{nJk} \boldsymbol{D}_{nJk}^{\text{in}}(\boldsymbol{r}) + \text{H.c.,} \qquad (3)$$

where b_{nJk} is the operator that annihilates an asymptotic-in photon associated with input channel n, with wave number k in the ring resonance J, and $\boldsymbol{D}_{nJk}^{\text{in}}(\boldsymbol{r})$ is the mode field associated with that photon [see the left sketch in Fig. 1(c) for the asymptotic-in mode field associated with the actual input channel]. Similarly, the displacement field operator can be written in terms of the asymptotic-out mode fields as

$$\boldsymbol{D}(\boldsymbol{r}) = \sum_{n,J} \int dk \, a_{nJk} \boldsymbol{D}_{nJk}^{\text{out}}(\boldsymbol{r}) + \text{H.c.,} \qquad (4)$$

where a_{nJk} is the operator that annihilates an asymptotic-out photon associated with output channel n, with wave number k in the ring resonance J, and $\boldsymbol{D}_{nJk}^{\text{out}}(\boldsymbol{r})$ is the mode field

associated with that photon [see the middle or right sketch in Fig. 1(c)]. The input and output operators satisfy the commutation relations

$$[a_{nJk}, a^{\dagger}_{nJk'}] = [b_{nJk}, b^{\dagger}_{nJk'}] = \delta(k - k'), \qquad (5)$$

with all others zero; the linear Hamiltonian can be written in terms of the input or output operators as

$$
\begin{aligned}
H_L &= \sum_{n,J} \int dk \, \hbar\omega_{nJk} b^{\dagger}_{nJk} b_{nJk} \\
&= \sum_{n,J} \int dk \, \hbar\omega_{nJk} a^{\dagger}_{nJk} a_{nJk},
\end{aligned}
\qquad (6)
$$

where ω_{nJk} is the dispersion relation for the waveguide containing channel n, ranging only over wave numbers k near ring resonance J (see Appendix A for details).

We now include a third-order nonlinear interaction described by the Hamiltonian [10]

$$H_{NL} = -\frac{1}{4\epsilon_0} \int d\boldsymbol{r} \, \Gamma_3^{ijkl}(\boldsymbol{r}) D^i(\boldsymbol{r}) D^j(\boldsymbol{r}) D^k(\boldsymbol{r}) D^l(\boldsymbol{r}), \qquad (7)$$

where i, j, k, and l are Cartesian components, as usual summed over when repeated, and the tensor $\Gamma_3^{ijkl}(\boldsymbol{r})$ is related to the more familiar third-order tensor $\chi_3^{ijkl}(\boldsymbol{r})$ by [10]

$$\Gamma_3^{ijkl}(\boldsymbol{r}) = \frac{\chi_3^{ijkl}(\boldsymbol{r})}{\epsilon_0^2 \epsilon^4(\boldsymbol{r})}, \qquad (8)$$

where we have assumed that the relative dielectric function $\epsilon(\boldsymbol{r})$ does not depend on frequency over the range of frequencies within each ring resonance and have neglected any dependence of $\chi_3^{ijlk}(\boldsymbol{r})$ over the frequencies of interest.

Our process of interest is SFWM, where one pump photon in resonance P and one in resonance C are annihilated and two photons in resonance S are generated [see Fig. 1(a)]. The asymptotic-out fields for the actual and phantom waveguides are used for the generated photons, while only the asymptotic-in mode field for the actual waveguide is used for the pump photons; hence we can drop the index n on the asymptotic-in mode fields and operators, understanding the actual input channel to be identified. If we consider only the terms responsible for SFWM in Eq. (7), the nonlinear Hamiltonian becomes [21]

$$
\begin{aligned}
H_{NL} = -\frac{3}{\epsilon_0} \sum_{n,n'} \int dk_1 dk_2 dk_3 dk_4 K^{nn'}(k_1, k_2, k_3, k_4) \\
\times \, a^{\dagger}_{nSk_1} a^{\dagger}_{n'Sk_2} b_{Pk_3} b_{Ck_4} + \text{H.c.},
\end{aligned}
\qquad (9)
$$

where the nonlinear coefficient for SFWM is given by

$$
\begin{aligned}
K^{nn'}(k_1, k_2, k_3, k_4) = \int d\boldsymbol{r} \, \Gamma_3^{ijkl}(\boldsymbol{r}) \big[D^{\text{out},i}_{nSk_1}(\boldsymbol{r}) \big]^* \\
\times \big[D^{\text{out},j}_{n'Sk_2}(\boldsymbol{r}) \big]^* D^{\text{in},k}_{Pk_3}(\boldsymbol{r}) D^{\text{in},l}_{Ck_4}(\boldsymbol{r}).
\end{aligned}
\qquad (10)
$$

The sums over n and n', which range over the actual and phantom output channels, take into account the four combinations of two photons exiting the ring through two output channels. More specifically, both photons can leave through the phantom or actual output channel, or one through each of the channels. The nonlinear coefficient $K^{nn'}(k_1, k_2, k_3, k_4)$

gives the strength of the interaction corresponding to each combination. It is symmetric with respect to exchanging the order of both n and n' and k_1 and k_2, that is,

$$K^{nn'}(k_1, k_2, k_3, k_4) = K^{n'n}(k_2, k_1, k_3, k_4), \qquad (11)$$

but it is not symmetric with respect to only exchanging the order of n and n' or k_1 and k_2, that is,

$$K^{nn'}(k_1, k_2, k_3, k_4) \neq K^{n'n}(k_1, k_2, k_3, k_4). \qquad (12)$$

We have derived the SFWM nonlinear coefficient in Eq. (10) considering the specific system of a ring resonator point coupled to two waveguides. In Appendix A we work out the nonlinear coefficient using the asymptotic-field mode profiles for the ring system in the expression (10) for the nonlinear coefficient and integrating over the ring where the fields are strongest; the resonant field enhancement in ring resonator systems is an advantage of ring resonator systems over the nonlinear waveguides that have been studied previously [12]. Moreover, our approach includes multiple modes of the asymptotic fields over a range of values of k, advancing previous single-mode treatments for three-wave interactions [13]. However, our approach is not limited to resonate systems. One of its strengths is that it can be used to study a general system that includes a nonlinear interaction, such as SFWM in a waveguide, simply by putting the asymptotic-field mode profiles for that system into the nonlinear coefficient in Eq. (10). Of course for an alternative system the number of input and output channels n can be different, but this is straightforward to accommodate.

III. INPUT AND OUTPUT KETS

The unitary time-evolution operator for the system, $\mathcal{U}(t, t')$, is a solution to the Schrödinger equation

$$i\hbar \frac{d\mathcal{U}(t, t')}{dt} = H\mathcal{U}(t, t'), \qquad (13)$$

satisfying $\mathcal{U}(t', t') = I$ for all t', where I is the identity operator. We write the full Hamiltonian H as the sum of the linear and nonlinear contributions

$$H = H_L + H_{NL}, \qquad (14)$$

where H_L is given by Eq. (6) and H_{NL} is given by Eq. (9). We assume that times t_{on} and t_{off} can be identified such that (a) for $t < t_{\text{on}}$ the excitations of the quantum fields incident on the ring are sufficiently far from it that H_{NL} has no effect on the evolution of the ket and (b) for $t > t_{\text{off}}$ all the field excitation has propagated sufficiently far from the ring that, again, H_{NL} has no effect on the evolution of the ket.

Consider then the evolution of a ket from some early time $t_0 < t_{\text{on}}$ to some later time $t_1 > t_{\text{off}}$. The evolution operator can be written as

$$\mathcal{U}(t_1, t_0) = \mathcal{U}(t_1, t_{\text{off}})\mathcal{U}(t_{\text{off}}, t_{\text{on}})\mathcal{U}(t_{\text{on}}, t_0). \qquad (15)$$

The evolution operator from t_0 to t_{on} and t_{off} to t_1 only involves the linear Hamiltonian, that is,

$$\mathcal{U}(t_{\text{on}}, t_0) = e^{-iH_L(t_{\text{on}} - t_0)/\hbar}, \qquad (16)$$

$$\mathcal{U}(t_1, t_{\text{off}}) = e^{-iH_L(t_1 - t_{\text{off}})/\hbar}. \qquad (17)$$

We can then write Eq. (15) as

$$\mathcal{U}(t_1, t_0) = e^{-iH_L(t_1-t_{\text{off}})/\hbar} \mathcal{U}(t_{\text{off}}, t_{\text{on}}) e^{-iH_L(t_{\text{on}}-t_0)/\hbar}. \quad (18)$$

We now suppose that an initial ket $|\psi(t_0)\rangle$ is specified at a time $t_0 < t_{\text{on}}$. We define the input ket

$$|\psi_{\text{in}}\rangle \equiv e^{-iH_L(0-t_0)/\hbar}|\psi(t_0)\rangle, \quad (19)$$

which is the ket that the initial ket would evolve to at $t = 0$ were $H_{NL} = 0$. In addition, starting with the ket $|\psi(t_1)\rangle$ characterizing the state at a time $t_1 > t_{\text{off}}$, we define the output ket

$$|\psi_{\text{out}}\rangle \equiv e^{iH_L(t_1-0)/\hbar}|\psi(t_1)\rangle, \quad (20)$$

which is the ket at $t = 0$ that would evolve to $|\psi(t_1)\rangle$ at $t = t_1$ were $H_{NL} = 0$. Since the evolution of the ket from from t_0 to t_1 is given by

$$|\psi(t_1)\rangle = \mathcal{U}(t_1, t_0)|\psi(t_0)\rangle, \quad (21)$$

in terms of the input and output kets this can be written as

$$|\psi_{\text{out}}\rangle = U(t_1, t_0)|\psi_{\text{in}}\rangle, \quad (22)$$

where we defined

$$U(t_1, t_0) \equiv e^{iH_L t_1/\hbar} \mathcal{U}(t_1, t_0) e^{-iH_L t_0/\hbar}. \quad (23)$$

Then taking the limit

$$U(\infty, -\infty) = \lim_{t_1 \to \infty, t_0 \to -\infty} U(t_1, t_0), \quad (24)$$

we obtain

$$|\psi_{\text{out}}\rangle = U(\infty, -\infty)|\psi_{\text{in}}\rangle. \quad (25)$$

It is then convenient to define

$$\bar{U}(t) \equiv U(t, -\infty) \quad (26)$$

for all times t. We can then write

$$|\psi_{\text{out}}\rangle = |\bar{\psi}(\infty)\rangle, \quad (27)$$

where

$$|\bar{\psi}(t)\rangle = \bar{U}(t)|\psi_{\text{in}}\rangle \quad (28)$$

and

$$|\psi_{\text{in}}\rangle = |\bar{\psi}(-\infty)\rangle. \quad (29)$$

Taking the derivative of Eq. (28) and using Eqs. (13), (23), and (26), we obtain

$$i\hbar \frac{d}{dt}|\bar{\psi}(t)\rangle = \bar{H}_{NL}(t)|\bar{\psi}(t)\rangle, \quad (30)$$

where we have defined the interaction picture nonlinear Hamiltonian as

$$\bar{H}_{NL}(t) \equiv e^{iH_L t/\hbar} H_{NL} e^{-iH_L t/\hbar}, \quad (31)$$

and as t ranges from $-\infty$ to ∞ in Eq. (30) the ket evolves from $|\psi_{\text{in}}\rangle$ to $|\psi_{\text{out}}\rangle$.

IV. UNITARY EVOLUTION

In Appendix A we simplify the nonlinear Hamiltonian (31) by treating the strong cw pump classically and discretize the k

involved for the weak pump and generated fields to implement numerical calculations. The result can be written as

$$\bar{H}_{NL}(t) = \hbar \sum_{\mu, \nu} \sum_l \Lambda_{\mu\nu l}(t) a_\mu^\dagger a_\nu^\dagger b_l + \text{H.c.}, \quad (32)$$

where for convenience we removed the discrete labels P and S on the input and output operators and they satisfy the usual commutation relations $[b_l, b_{l'}^\dagger] = \delta_{ll'}$ and $[a_\mu, a_\nu^\dagger] = \delta_{\mu\nu}$. Here $\Lambda_{\mu\nu l}(t)$ is the nonlinear coefficient for the effective $\chi^{(2)}$ interaction, where l labels a discrete wave number k_l for the pump, and μ and ν are discrete indices for the generated photons [see Eq. (A14)]. Each greek index μ, for example, refers to two properties of the photon, its discrete wave number k_i and the output channel n. The sum over μ in Eq. (32) represents two sums, one over the actual and phantom output channel and the second over the discrete wave numbers k_i.

We now turn to the unitary evolution in Eq. (30). Here we do not consider a general initial ket $|\psi(t_0)\rangle$ at the initial time t_0, but restrict ourselves to an initial ket that is a coherent state for the pump in the actual input channel and vacuum in all other channels,

$$|\psi(t_0)\rangle = D_b(e^{-i\boldsymbol{\omega}_P t_0}\boldsymbol{\beta}_{\text{in}})|\text{vac}\rangle, \quad (33)$$

where $D_b(e^{-i\boldsymbol{\omega}_P t_0}\boldsymbol{\beta}_{\text{in}})$ is the unitary displacement operator given by

$$D_b(e^{-i\boldsymbol{\omega}_P t_0}\boldsymbol{\beta}_{\text{in}}) = \exp[(e^{-i\boldsymbol{\omega}_P t_0}\boldsymbol{\beta}_{\text{in}})^T \boldsymbol{b}^\dagger - (e^{i\boldsymbol{\omega}_P t_0}\boldsymbol{\beta}_{\text{in}}^*)^T \boldsymbol{b}], \quad (34)$$

where the subscript b corresponds to the input operators for the pump, and $\boldsymbol{b} = [b_1, b_2, \ldots]^T$ and $\boldsymbol{b}^\dagger = [b_1^\dagger, b_2^\dagger, \ldots]^T$ are column vectors of input operators. Here $\boldsymbol{\omega}_P$ is the dispersion relation for the pump in the input channel of the actual waveguide. It is written as a diagonal matrix $\boldsymbol{\omega}_P = \text{diag}(\omega_{P,1}, \omega_{P,2}, \ldots)$, where $\omega_{P,l}$ is the frequency of the pump mode with discrete wave number k_l, and $\boldsymbol{\beta}_{\text{in}} = [\beta_{\text{in},1}, \beta_{\text{in},2}, \ldots]^T$ is a column vector of initial displacement parameters. For example, in Sec. VI we take $\boldsymbol{\beta}_{\text{in}}$ to have a Gaussian distribution. Putting Eq. (33) for $|\psi(t_0)\rangle$ into Eq. (19) for $|\psi_{\text{in}}\rangle$, the input ket can be written as

$$|\psi_{\text{in}}\rangle = \exp([\boldsymbol{\beta}_{\text{in}}]^T \boldsymbol{b}^\dagger - [\boldsymbol{\beta}_{\text{in}}^*]^T \boldsymbol{b})|\text{vac}\rangle, \quad (35)$$

where we used the linear Hamiltonian in Eq. (6).

We then seek a solution of Eq. (30) of the form

$$|\bar{\psi}(t)\rangle = U_a(t) U_b(t)|\tilde{\psi}(t)\rangle, \quad (36)$$

where $|\tilde{\psi}(t)\rangle$ describes the effect of a non-Gaussian unitary operator acting on the vacuum state, as discussed below, and $U_a(t)$ and $U_b(t)$ are Gaussian unitary operators, given by

$$U_a(t) = S_a[\boldsymbol{J}(t)] R_a[\boldsymbol{\phi}(t)] e^{i\theta_a(t)}, \quad (37)$$

$$U_b(t) = D_b[\boldsymbol{\beta}(t)] e^{i\theta_b(t)}, \quad (38)$$

where $\theta_b(t)$ and $\theta_a(t)$ are real functions of time, $S_a[\boldsymbol{J}(t)]$ is a multimode squeezing operator, $R_a[\boldsymbol{\phi}(t)]$ is a multimode rotation operator, and $D_b[\boldsymbol{\beta}(t)]$ is the multimode displacement operator that has the same form as Eq. (34). Here the subscript a corresponds to the output operators for the generated squeezed light and as above the subscript b corresponds to the input operators for the pump.

The unitary squeezing operator $S_a[\boldsymbol{J}(t)]$ is given by [22]

$$S_a[\boldsymbol{J}(t)] = \exp[\tfrac{1}{2}\boldsymbol{a}^{\dagger\mathrm{T}}\boldsymbol{J}(t)\boldsymbol{a}^\dagger - \mathrm{H.c.}], \qquad (39)$$

where $\boldsymbol{a} = [a_1, a_2, \ldots]^\mathrm{T}$ and $\boldsymbol{a}^\dagger = [a_1^\dagger, a_2^\dagger, \ldots]^\mathrm{T}$ are column vectors of output operators and $\boldsymbol{J}(t)$ is the symmetric time-dependent squeezing matrix, with $\boldsymbol{J}(t) = \boldsymbol{J}^\mathrm{T}(t)$. The unitary rotation operator $R_a[\boldsymbol{\phi}(t)]$ is given by [22]

$$R_a[\boldsymbol{\phi}(t)] = \exp[i\boldsymbol{a}^{\dagger\mathrm{T}}\boldsymbol{\phi}(t)\boldsymbol{a}], \qquad (40)$$

where $\boldsymbol{\phi}(t)$ is the Hermitian time-dependent rotation matrix, with $\boldsymbol{\phi}(t) = \boldsymbol{\phi}^\dagger(t)$. The parameters $\boldsymbol{\beta}(t)$, $\boldsymbol{J}(t)$, and $\boldsymbol{\phi}(t)$ are subject to the following initial conditions $\boldsymbol{\beta}(-\infty) = \boldsymbol{\beta}_{\mathrm{in}}$, $\boldsymbol{J}(-\infty) = 0$, and $\boldsymbol{\phi}(-\infty) = 0$, and also $\theta_b(-\infty) = \theta_a(-\infty) = 0$; further, we take

$$|\tilde{\psi}(-\infty)\rangle = |\mathrm{vac}\rangle. \qquad (41)$$

This guarantees that the initial condition (29) is satisfied.

Returning to Eq. (36), our goal is to define the parameters in the Gaussian unitary operators in Eqs. (37) and (38) so that the ket $|\tilde{\psi}(t)\rangle$ isolates the non-Gaussian behavior of the full ket in Eq. (36). Now regardless of how the parameters in those Gaussian unitary operators are chosen to depend on time, we find that for Eq. (36) to satisfy the full Schrödinger equation (30) we require

$$i\hbar\frac{d}{dt}|\tilde{\psi}(t)\rangle = H_{\mathrm{eff}}(t)|\tilde{\psi}(t)\rangle, \qquad (42)$$

where we have introduced the effective Hamiltonian

$$H_{\mathrm{eff}}(t) = H_I(t) + U_a^\dagger(t)H_a(t)U_a(t) - i\hbar U_a^\dagger(t)\frac{dU_a(t)}{dt}$$
$$+ U_b^\dagger(t)H_b(t)U_b(t) - i\hbar U_b^\dagger(t)\frac{dU_b(t)}{dt}, \qquad (43)$$

with

$$H_a(t) \equiv \hbar\Lambda_{\mu\nu l}(t)[\boldsymbol{\beta}(t)]_l a_\mu^\dagger a_\nu^\dagger + \mathrm{H.c.}, \qquad (44)$$

$$H_b(t) \equiv \hbar\Lambda_{\mu\nu l}^*(t)[\boldsymbol{V}(t)\boldsymbol{W}^\mathrm{T}(t)]_{\mu\nu}\{b_l^\dagger - [\boldsymbol{\beta}^*(t)]_l\} + \mathrm{H.c.}, \qquad (45)$$

$$H_I(t) \equiv \hbar\Lambda_{\mu\nu l}^*(t)([\boldsymbol{V}(t)]_{\mu\mu'}[\boldsymbol{V}(t)]_{\nu\nu'}a_{\mu'}a_{\nu'}$$
$$+ \{[\boldsymbol{V}(t)]_{\mu\nu'}[\boldsymbol{W}(t)]_{\nu\mu'} + [\boldsymbol{W}(t)]_{\mu\mu'}[\boldsymbol{V}(t)]_{\nu\nu'}\}a_{\mu'}^\dagger a_{\nu'}$$
$$+ [\boldsymbol{W}(t)]_{\mu\mu'}[\boldsymbol{W}(t)]_{\nu\nu'}a_{\mu'}^\dagger a_{\nu'}^\dagger)b_l^\dagger + \mathrm{H.c.} \qquad (46)$$

Here repeated indices are summed over, and the matrices $\boldsymbol{V}(t)$ and $\boldsymbol{W}(t)$ are defined in terms of the parameters appearing in the Gaussian unitary operators in Eqs. (37) and (38) (see Appendix B for details).

The Hamiltonians appearing above each capture part of the physics: $H_a(t)$ describes the generation of photon pairs by an effective $\chi^{(2)}$ interaction modulated by a time-dependent pump amplitude $\boldsymbol{\beta}(t)$; $H_b(t)$ determines the rate of depletion of the pump amplitude $\boldsymbol{\beta}(t)$, which is being driven by the generation of photon pairs; $H_I(t)$, which only contains non-Gaussian terms, describes the quantum correlations between the pump and the generated light.

To achieve our goal of moving all the non-Gaussian behavior to $|\tilde{\psi}(t)\rangle$, we must choose the time dependence of the parameters appearing in the Gaussian operators in Eqs. (37) and (38) so that

$$H_{\mathrm{eff}}(t) = H_I(t). \qquad (47)$$

It is easy to show that this condition is satisfied if we have

$$i\hbar\frac{dU_a(t)}{dt} = H_a(t)U_a(t), \qquad (48)$$

$$i\hbar\frac{dU_b(t)}{dt} = H_b(t)U_b(t). \qquad (49)$$

We show in Appendix B that this can be achieved by appropriately choosing the parameters $\boldsymbol{V}(t)$, $\boldsymbol{W}(t)$, $\boldsymbol{\beta}(t)$, and $\theta_b(t)$ so that

$$\frac{d\boldsymbol{V}(t)}{dt} = -2i\boldsymbol{\zeta}(t)\boldsymbol{W}^*(t), \qquad (50)$$

$$\frac{d\boldsymbol{W}(t)}{dt} = -2i\boldsymbol{\zeta}(t)\boldsymbol{V}^*(t), \qquad (51)$$

$$i\frac{d[\boldsymbol{\beta}(t)]_l}{dt} = [\boldsymbol{\gamma}(t)]_l, \qquad (52)$$

$$\theta_b(t) = \frac{1}{2}\int_{-\infty}^t dt'[\boldsymbol{\gamma}(t')]_l[\boldsymbol{\beta}^*(t')]_l + \mathrm{c.c.} \qquad (53)$$

are satisfied, where the matrix $\boldsymbol{\zeta}(t)$ drives the production of photon pairs in the squeezed state,

$$[\boldsymbol{\zeta}(t)]_{\mu\nu} = \Lambda_{\mu\nu l}(t)[\boldsymbol{\beta}(t)]_l, \qquad (54)$$

and the vector $\boldsymbol{\gamma}(t)$ determines the rate of pump depletion,

$$[\boldsymbol{\gamma}(t)]_l = \Lambda_{\mu\nu l}^*(t)[\boldsymbol{V}(t)\boldsymbol{W}^\mathrm{T}(t)]_{\mu\nu}. \qquad (55)$$

We solve Eqs. (50), (51), and (52) numerically for the parameters $\boldsymbol{V}(t)$, $\boldsymbol{W}(t)$, and $\boldsymbol{\beta}(t)$, respectively, which are subject to the initial conditions $\boldsymbol{\beta}(-\infty) = \boldsymbol{\beta}_{\mathrm{in}}$, $\boldsymbol{W}(-\infty) = 0$, and $\boldsymbol{V}(-\infty) = \boldsymbol{I}$ [see Eq. (29)], where $\boldsymbol{I}$ is the identity matrix. The solutions are put into Eq. (53), which is then integrated to obtain the phase $\theta_b(t)$. In Appendix C we show how to extract the squeezing matrix $\boldsymbol{J}(t)$ and rotation matrix $\boldsymbol{\phi}(t)$ from the solutions $\boldsymbol{V}(t)$ and $\boldsymbol{W}(t)$, and in Appendix D we give an equation for the phase $\theta_a(t)$ in Eq. (37). This procedure provides a solution for the Gaussian parameters of the unitary operators in Eqs. (37) and (38) and is valid for high pump power and nonlinear interaction strength.

Still necessary for a full solution, of course, is to include the non-Gaussian evolution of $|\tilde{\psi}(t)\rangle$. Then the full solution can be written as a squeezed, displaced, and rotated version of the non-Gaussian ket $|\tilde{\psi}(t)\rangle$, as given in Eq. (36). An attractive feature of this approach is that we can work in the Gaussian limit by setting $|\tilde{\psi}(t)\rangle \to |\mathrm{vac}\rangle$ in Eq. (36) and still study the effects of pump depletion and the dynamics of the joint spectral amplitude in squeezed-state generation.

That is what we do for the remainder of this paper. We put

$$|\tilde{\psi}(t)\rangle \to U_a(t)U_b(t)|\mathrm{vac}\rangle \equiv |\bar{\psi}_G(t)\rangle, \qquad (56)$$

and we have

$$|\bar{\psi}_G(t)\rangle = e^{i\theta_a(t)}S_a[\boldsymbol{J}(t)]|\mathrm{vac}\rangle \otimes e^{i\theta_b(t)}|\boldsymbol{\beta}(t)\rangle, \qquad (57)$$

where $|\boldsymbol{\beta}(t)\rangle = D_b[\boldsymbol{\beta}(t)]|\mathrm{vac}\rangle$ is a coherent state. The Gaussian state is a product of a squeezed vacuum state written in terms of the output operators and a coherent state written in

terms of the input operators, and from Eq. (56) its dynamics is governed by

$$i\hbar \frac{d|\bar{\psi}_G(t)\rangle}{dt} = [H_a(t) + H_b(t)]|\bar{\psi}_G(t)\rangle. \tag{58}$$

The Gaussian state approximation neglects the entanglement between the pump and the squeezed state. However, this entanglement can be a significant characteristic of the full state if the coefficients in the non-Gaussian Hamiltonian $H_I(t)$ in Eq. (46) are non-negligible. To examine the validity of the Gaussian approximation for our problem, we consider a perturbative solution to Eq. (42), assuming that $H_I(t)$ is small,

$$|\tilde{\psi}(t)\rangle \approx |\text{vac}\rangle + |\tilde{\psi}_1(t)\rangle + \cdots, \tag{59}$$

where

$$|\tilde{\psi}_1(t)\rangle = F_{l\mu'\nu'}(t)a_{\mu'}^\dagger a_{\nu'}^\dagger b_l^\dagger|\text{vac}\rangle, \tag{60}$$

with

$$F_{l\mu'\nu'}(t) = -i \int_{-\infty}^t dt' \Lambda_{\mu\nu l}^*(t')[\boldsymbol{W}(t')]_{\mu\mu'}[\boldsymbol{W}(t')]_{\nu\nu'}, \tag{61}$$

where the second term in Eq. (59) results from the only term in $H_I(t)$ that does not destroy the vacuum ket. For the Gaussian approximation $|\tilde{\psi}(t)\rangle \approx |\text{vac}\rangle$ to be a good one, we require

$$\langle\tilde{\psi}_1(\infty)|\tilde{\psi}_1(\infty)\rangle \ll 1. \tag{62}$$

Generally, this condition will not be satisfied if the elements of the tensor $\Lambda_{\mu\nu l}(t)$ are large or the number of squeezed photons, given by $\text{tr}[\boldsymbol{W}^*(t)\boldsymbol{W}^\text{T}(t)]$ [10], is a significant fraction of the number of pump photons. However, in Sec. VI we show that this condition is satisfied for the squeezed state generated by an effective second-order interaction in a silicon nitride ring resonator with the pump powers and parameters we consider.

There is an additional consequence of the Gaussian approximation: The operator $Q = \boldsymbol{a}^{\dagger\text{T}}\boldsymbol{a}/2 + \boldsymbol{b}^{\dagger\text{T}}\boldsymbol{b}$ commutes with H_L and H_{NL} and therefore with the full Hamiltonian in Eq. (14), and so is a conserved quantity. It therefore also commutes with $\bar{H}_{NL}(t)$, which governs the evolution of the full $|\bar{\psi}(t)\rangle$ according to Eq. (30). However, it does *not* commute with the Hamiltonian $H_a(t) + H_b(t)$ that governs the evolution of the Gaussian approximation ket $|\bar{\psi}_G(t)\rangle$. Thus, under the Gaussian approximation the operator Q is not a conserved quantity. Nonetheless, in Appendix E we show that its expectation value in the Gaussian approximation, $\langle\bar{\psi}_G(t)|Q|\bar{\psi}_G(t)\rangle$ *is* constant as $|\bar{\psi}_G(t)\rangle$ evolves according to Eq. (58).

V. FIRST-ORDER SOLUTION

If the energy of the pump is sufficiently low or the nonlinear coefficients $\Lambda_{\mu\nu l}(t)$ are sufficiently weak, then the elements of the matrix $\boldsymbol{\zeta}(t)$ in Eq. (54) will be much less than unity, $[\boldsymbol{\zeta}(t)]_{\mu\nu} \ll 1$ for all μ and ν. In this case the solution to Eqs. (50) and (51) can be approximately written as [10]

$$\boldsymbol{V}(t) \approx \boldsymbol{I}, \tag{63}$$

$$\boldsymbol{W}(t) \approx -2i \int_{-\infty}^t dt' \boldsymbol{\zeta}(t'). \tag{64}$$

Consequently, the pump depletion rate in Eq. (52) is negligible

$$\frac{d[\boldsymbol{\beta}(t)]_l}{dt} \approx -2i\Lambda_{\mu\nu l}^*(t) \int_{-\infty}^t dt' [\boldsymbol{\zeta}(t')]_{\mu\nu} \approx 0, \tag{65}$$

since it depends on the product of the nonlinear coefficients, which are assumed to be small. The Hamiltonian $H_b(t)$ in Eq. (45) can be set to zero, $H_b(t) \to 0$, since the coefficients in $H_b(t)$ are given by $d[\boldsymbol{\beta}(t)]_l/dt$. Similarly, the phase $\theta_b(t)$ in Eq. (53) is negligible, $\theta_b(t) \approx 0$.

With these approximations, the Gaussian ket $|\bar{\psi}_G(t)\rangle$ in Eq. (57) can be written as

$$|\bar{\psi}_G(t)\rangle = S_a[\boldsymbol{J}(t)]|\text{vac}\rangle \otimes |\boldsymbol{\beta}_{\text{in}}\rangle, \tag{66}$$

which satisfies the Schrödinger equation

$$i\hbar \frac{d|\bar{\psi}_G(t)\rangle}{dt} = H_a(t)|\bar{\psi}_G(t)\rangle. \tag{67}$$

Treating $H_a(t)$ as a small quantity, we can construct a first-order solution to Eq. (67) using the Magnus expansion [8], and keeping only the first term, we obtain

$$|\bar{\psi}_G(t)\rangle \approx \exp\left(-i \int_{-\infty}^t dt' [\boldsymbol{\zeta}(t')]_{\mu\nu} a_\mu^\dagger a_\nu^\dagger - \text{H.c.}\right) \otimes |\boldsymbol{\beta}_{\text{in}}\rangle. \tag{68}$$

The higher-order terms in the expansion involve the commutator between the Hamiltonian at two different times, such as $[H_a(t), H_a(t')]$ [8]. The ket in Eq. (68) is the solution when we assume that $[H_a(t), H_a(t')] = 0$ so that time-ordering effects are negligible. It was pointed out earlier for waveguides [10,12] that this assumption becomes invalid when the power of the pump is increased. We demonstrate below that this also holds for a squeezed state generated in a ring resonator. Comparing Eqs. (68) and (66), we immediately obtain the approximate first-order solution for the squeezing matrix

$$\boldsymbol{J}(t) \approx -2i \int_{-\infty}^t dt' \boldsymbol{\zeta}(t'). \tag{69}$$

This is the expression for $\boldsymbol{W}(t)$ in Eq. (64), so we can write $\boldsymbol{J}(t) \approx \boldsymbol{W}(t)$. To obtain the form in Eq. (66) we set $\theta_a(t) = 0$, which is valid for a weak nonlinearity (see Appendix D).

VI. EXAMPLE: SQUEEZED-STATE GENERATION IN A RING RESONATOR

In this section we study the example of generating a highly squeezed state in a ring resonator. We calculate the squeezing matrix, the number of generated photons, the Schmidt number, and the second-order correlation function in the actual output channel including scattering loss and compare these results to the first-order solution.

We consider a SiN ring resonator point coupled to an actual waveguide and a phantom waveguide, the latter modeling scattering loss [see Fig. 1(b)]. We consider a structure similar to that considered by Vernon *et al.* [20], with a ring radius of $R = 64$ μm, $\omega_S = 2\pi \times 193$ THz, a group velocity of 1.5×10^8 m/s, a nonlinear parameter of $\bar{\gamma}_{NL} \approx 1$ $(\text{W m})^{-1}$ [see Eq. (A13)], and an intrinsic quality factor of 2×10^6 for all three ring resonances. We take the loaded quality factors for the P, S, and C modes to be 4×10^4 (overcoupled),
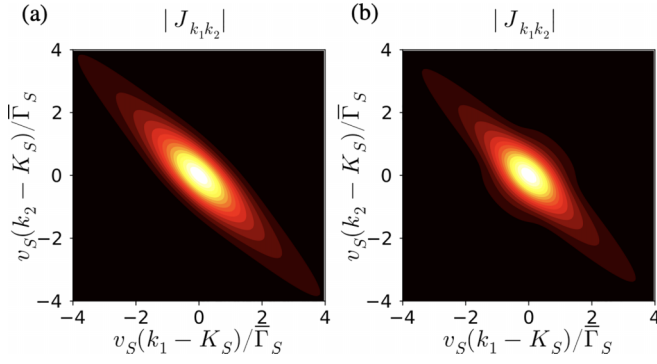
FIG. 2. Magnitude of the elements of the squeezing matrix $|J_{k_1 k_2}|$ in the strong pump regime ($U_P = 100$ pJ) calculated using the (a) first-order solution and (b) the full numerical Gaussian solution.

2×10^5 (overcoupled), and 1×10^6 (critically coupled), respectively.

In mode C there is an undepleted cw pump with power $P_C = 30$ mW, and in mode P there is a weak pulsed pump with energy U_P and duration $\tau_P = 0.5$ ns. The initial amplitude of the pulse is

$$[\boldsymbol{\beta}_{\text{in}}]_l = \sqrt{\frac{N_P v_P \tau_P}{\sqrt{\pi}}} \exp\left[-\tfrac{1}{2}(k_l - K_P)^2 v_P^2 \tau_P^2\right], \quad (70)$$

where for simplicity we neglect group velocity dispersion, N_P is the initial photon number, v_p is the group velocity, and K_P is the central wave number.

In Figs. 2(a) and 2(b) we plot the magnitude of the components $J_{k_1 k_2}$ of the final squeezing matrix $\boldsymbol{J}(\infty)$ for $U_P = 100$ pJ ($N_P \approx 7.8 \times 10^8$). The x axes and y axes of Figs. 2(a) and 2(b) represent the detuning from the center of the ring resonance of the mode S, where v_S, K_S, and $1/\bar{\Gamma}_S \approx 330$ ps are its group velocity, central wave number, and dwelling time, respectively. In Fig. 2(a) we show the scattering matrix $\boldsymbol{J}(\infty)$ as predicted by the first-order solution of Eq. (69); in Fig. 2(b) we show the solution using the full Gaussian solution in Eq. (C20) found by numerically solving the coupled differential equations (50)–(52). The full Gaussian solution in Fig. 2(b) exhibits less correlation between the wave numbers k_1 and k_2 of the generated photon pairs than the first-order solution in Fig. 2(a). For this energy the first-order solution predicts an average generated photon number of about 11, which corresponds to approximately 16.7 dB of squeezing; in the full Gaussian calculation the average generated photon number is about 19, which corresponds to approximately 19 dB of squeezing.

In Fig. 3(a) the average generated photon number in the squeezed state is shown for pump energy U_P between 1 and 100 pJ. The calculations are done with the full Gaussian solution (blue solid line) and the first-order solution (pink dashed line). The photon number is calculated with tr$[\boldsymbol{W}^*(t)\boldsymbol{W}^{\text{T}}(t)]$ [10], where the matrix $\boldsymbol{W}(t)$ is obtained using the full Gaussian solution or the first-order solution. The first-order solution gives a photon number that is smaller than that of the full Gaussian solution by approximately 20% or less for pump energies at or below 60 pJ. This corresponds to an underestimation of the squeezing by about 1 dB at
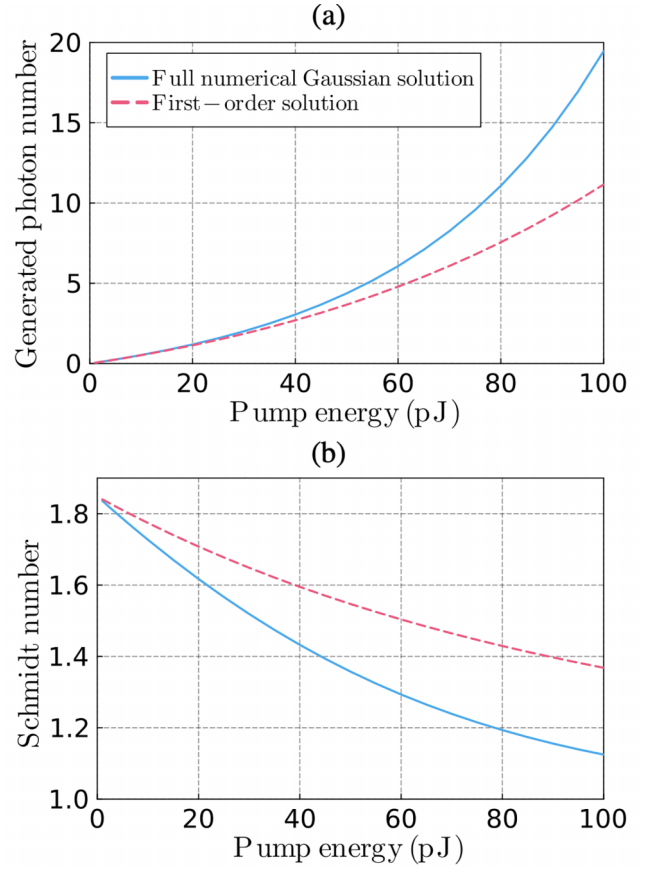

FIG. 3. (a) Average generated photon number in the squeezed state and (b) Schmidt number, calculated with the full numerical Gaussian solution (blue solid line) and the first-order solution (pink dashed line) for increasing energy of the pulsed pump (U_P).

most. However, at 80 and 100 pJ the first-order solution underestimates the squeezing by 1.6 and 2.3 dB, respectively.

Despite the high level of squeezing, the level of pump depletion is negligible. As a result, we expect the neglect of the non-Gaussian corrections to the vacuum, which are captured by the evolution (42) of $|\tilde{\psi}(t)\rangle$ and which we expect to only become important when there is significant pump depletion [12], is justified. To confirm it is reasonable to neglect the non-Gaussian corrections we calculate

$$\langle \tilde{\psi}_1(\infty)|\tilde{\psi}_1(\infty)\rangle = 2F_{l\mu'\nu'}(\infty)F^*_{l\mu'\nu'}(\infty) \quad (71)$$

for a high pump energy of $U_P = 100$ pJ and find it is on the order of 10^{-8}; thus Eq. (62) is well satisfied.

For the same parameters as adopted above, in Fig. 3(b) we show the Schmidt number [23] of the squeezing matrix $\boldsymbol{J}(t)$. It is given by

$$K_S(t) = \frac{\left(\sum_j \sinh^2[r_j(t)]\right)^2}{\sum_j \sinh^4[r_j(t)]}, \quad (72)$$

where the $r_j(t)$, for $j = 1, 2, \ldots$, are the singular values obtained from a singular value decomposition (SVD) of $\boldsymbol{J}(t)$. A Schmidt number of unity $K_S(t) = 1$ indicates that $\boldsymbol{J}(t)$ has only one singular value and the squeezed state can be written as a single-mode squeezed state in terms of a single Schmidt

mode. A Schmidt number greater than unity $K_S(t) > 1$ indicates that the squeezed state is characterized by multiple Schmidt modes. In Fig. 3(b) the Schmidt number of $\boldsymbol{J}(t)$ is calculated using the first-order solution and the full Gaussian solution. The first-order solution consistently overestimates the Schmidt number, and thus the squeezed state obtained from the full Gaussian solution is more single mode than what is predicted by the first-order solution.

Each Schmidt mode typically involves light exiting into both the actual and the phantom waveguide, the latter modeling the scattering of light off the chip. In order to study the temporal correlations between the generated photon pairs that both exit the output channel of the actual waveguide, we consider a measurement of the second-order correlation function $G^{(2)}(t_1, t_2)$ of the squeezed light exiting the actual output channel. It is convenient to introduce a channel operator $\bar{a}(x, t)$ as the Fourier transform of the output operators for the actual waveguide a_k as [24]

$$\bar{a}(x, t) = \int \frac{dk}{\sqrt{2\pi}} a_k e^{i(k-K_S)(x-v_S t)}, \tag{73}$$

where x is the direction of propagation in the waveguide. The operator $\bar{a}(x, t)$ is associated with an electric field at the position x and time t. Just beyond the coupling point between the ring and waveguide ($x = 0^+$), the second-order correlation function is given by [25]

$$G^{(2)}(t_1, t_2) = v_S^2 \langle \bar{a}^\dagger(0^+, t_1) \bar{a}^\dagger(0^+, t_2) \bar{a}(0^+, t_2) \bar{a}(0^+, t_1) \rangle, \tag{74}$$

where the expectation value is done with the Gaussian ket in Eq. (57). This can be used to predict the probability of detecting coincidence counts at the two times t_1 and t_2. We normalize it using Φ^2, where Φ is the ratio of the number of generated photons per pump pulse duration, given by

$$\Phi \equiv \langle n_S \rangle / \tau_P, \tag{75}$$

where $\langle n_S \rangle$ is the number of generated photons.

In Figs. 4(a) and 4(b) we show the second-order correlation function for the actual output channel, calculated using the first-order solution, and in Figs. 4(c) and 4(d) we show it as calculated using the full Gaussian solution. When the energy of the pump pulse is 10 pJ the correlation functions from the first-order solution and full Gaussian solution appear to agree. However, for the high-energy pump pulse at 100 pJ, the first-order solution begins to show correlations that are not present in the full Gaussian solution, and the maximum of the first-order solution occurs at an earlier time ($t_1 = t_2 = 0.9/\bar{\Gamma}_S$) than does that of the full Gaussian solution ($t_1 = t_1 = 1.5/\bar{\Gamma}_S$).

VII. CONCLUSION

We have presented a multimode theory of Gaussian state generation for an effective $\chi^{(2)}$ interaction, in terms of asymptotic-in and -out fields, that includes scattering loss and pump depletion. We showed that the full ket for our system can be written as a Gaussian unitary acting on non-Gaussian ket that satisfies a Schrödinger equation with an effective Hamiltonian that describes the quantum correlations between
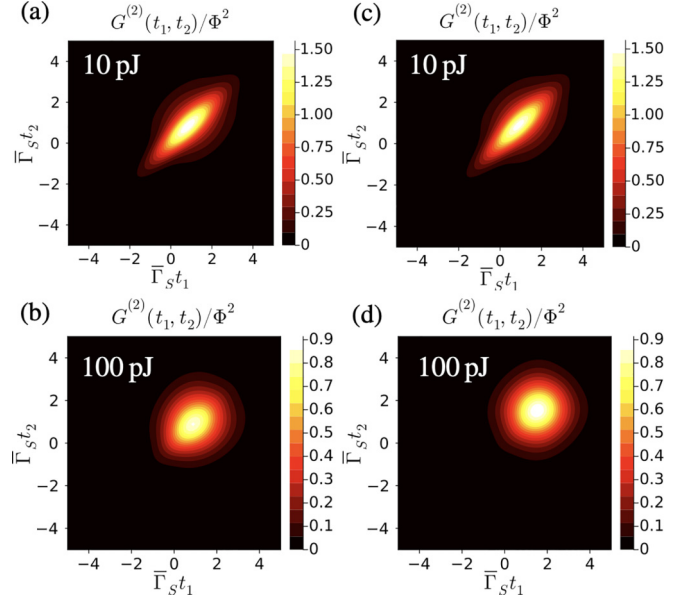

FIG. 4. Comparison of the second-order correlation functions $G^{(2)}(t_1, t_2)$ in the actual output channel using the first-order solution (left column) with (a) $U_P = 10$ pJ and (b) $U_P = 100$ pJ and using the full numerical Gaussian solution (right column) with (c) $U_P = 10$ pJ and (d) $U_P = 100$ pJ.

the pump and the generated light. In order for this to be valid, we required that the squeezing, rotation, and displacement parameters of the Gaussian unitary were solutions to a set of coupled differential equations. As an example we studied the lossy generation of a highly squeezed state using an effective $\chi^{(2)}$ interaction in a silicon nitride ring resonator and we compared this full Gaussian solution to a lowest-order Magnus expansion for the ket. We found that the amount of pump depletion in the ring was negligible, as was the first-order non-Gaussian correction term to the squeezed state. We leave for future work the study of the evolution of the non-Gaussian ket, the effects of self- and cross-phase modulation, and the application to more general resonant systems where the non-Gaussian corrections will be more significant. This work opens up a path to study the deterministic generation of non-Gaussian states in resonant systems.

APPENDIX A: EFFECTIVE $\chi^{(2)}$ INTERACTION IN A RING RESONATOR

In this Appendix we derive the nonlinear Hamiltonian for an effective $\chi^{(2)}$ interaction in a ring resonator.

We begin with the nonlinear Hamiltonian for SFWM in Eq. (9). In the interaction picture

it takes the form

$$\bar{H}_{NL}(t) = -\frac{3}{\epsilon_0} \sum_{n,n'} \int dk_1 dk_2 dk_3 dk_4$$
$$\times K^{nn'}(k_1, k_2, k_3, k_4) e^{-i\Omega_{nn'}(k_1,k_2,k_3,k_4)t}$$
$$\times a_{nSk_1}^\dagger a_{n'Sk_2}^\dagger b_{Pk_3} b_{Ck_4} + \text{H.c.}, \quad (A1)$$

where we have used the definition in Eq. (31) and defined

$$\Omega_{nn'}(k_1, k_2, k_3, k_4) \equiv \omega_{Ck_4} + \omega_{Pk_3} - \omega_{n'Sk_2} - \omega_{nSk_1}. \quad (A2)$$

In order to build the effective $\chi^{(2)}$ interaction, the pump in the mode C is treated classically with a cw field that is undepleted. The operators b_{Ck_4} are replaced with the amplitudes [21]

$$b_{Ck_4} \to \sqrt{\frac{2\pi P_C}{\hbar \omega_C v_C}} \delta(k_4 - K_C), \quad (A3)$$

where P_C is the cw power and v_C is the group velocity of the cw pump in the actual input channel. Under this approximation, Eq. (A1) becomes

$$\bar{H}_{NL}(t) = \hbar \sum_{n,n'} \int dk_1 dk_2 dk_3 \Lambda^{nn'}(k_1, k_2, k_3, t)$$
$$\times a_{nSk_1}^\dagger a_{n'Sk_2}^\dagger b_{Pk_3} + \text{H.c.}, \quad (A4)$$

where the effective $\chi^{(2)}$ coefficient $\Lambda^{nn'}(k_1, k_2, k_3, t)$ is given by

$$\Lambda^{nn'}(k_1, k_2, k_3, t) = -\frac{3}{\hbar\epsilon_0} \sqrt{\frac{2\pi P_C}{\hbar \omega_C v_C}} K^{nn'}(k_1, k_2, k_3, K_C)$$
$$\times e^{-i\Omega_{nn'}(k_1,k_2,k_3,K_C)t}. \quad (A5)$$

We consider a ring resonator that is point coupled to an actual waveguide that couples light both into and out of the ring and a phantom waveguide that handles the scattering loss [recall Fig. 1(b)]. The circumference of the ring is given by $\mathcal{L} = 2\pi R$, where R is its radius. The resonant wave numbers for the ring are given by κ such that $\kappa\mathcal{L} = 2\pi m$, where m is a positive integer. We assume that around each ring resonance we can neglect group velocity dispersion and that the dispersion relation is the same for the actual and phantom waveguides. Under these assumptions, the dispersion relation for either channel is given by

$$\omega_J(k) = \omega_J + v_J(k - K_J), \quad (A6)$$

where ω_J is the center frequency of the resonance J, v_J is the group velocity in either channel, and K_J is the wave number for the light in either channel with frequency ω_J. The linewidth of the ring resonances is given by $2\bar{\Gamma}_J$, which includes coupling losses to the actual waveguide and scattering losses to the phantom waveguide; the loaded quality factor is then $Q_J^{\text{load}} = \omega_J/2\bar{\Gamma}_J$.

The asymptotic-in and -out displacement fields are defined over all space, but we assume that the nonlinear interaction takes place mostly inside the ring resonator. Thus to obtain the nonlinear coefficient we only require expressions for the field that hold at positions in the ring. To simplify the integration of that region of space, we introduce the coordinates of the ring frame as $(\boldsymbol{r}_\perp, \zeta)$, where $\boldsymbol{r}_\perp = (\rho, z)$ and $\zeta = \phi R$, and (ρ, ϕ, z)

are cylindrical coordinates. For positions inside the ring, the asymptotic-in pump fields can be written as [21]

$$\boldsymbol{D}_{Pk}^{\text{in}}(\boldsymbol{r}) = -\sqrt{\frac{\hbar\omega_P}{4\pi}} \boldsymbol{d}_P(\boldsymbol{r}_\perp; \zeta) e^{i\zeta\kappa_P} F_{P-}(k), \quad (A7)$$

$$\boldsymbol{D}_{Ck}^{\text{in}}(\boldsymbol{r}) = -\sqrt{\frac{\hbar\omega_C}{4\pi}} \boldsymbol{d}_C(\boldsymbol{r}_\perp; \zeta) e^{i\zeta\kappa_C} F_{C-}(k) \quad (A8)$$

and the asymptotic-out fields can be written as

$$\boldsymbol{D}_{nSk}^{\text{out}}(\boldsymbol{r}) = -\sqrt{\frac{\hbar\omega_S}{4\pi}} \boldsymbol{d}_S(\boldsymbol{r}_\perp; \zeta) e^{i\zeta\kappa_S} F_{S+}^{(n)}(k). \quad (A9)$$

Here we introduced the field enhancement factors for the actual input channel, $F_{J-}(k)$, given by [21]

$$F_{J-}(k) = \frac{1}{\sqrt{\mathcal{L}}} \left(\frac{(\gamma_J)^*}{v_J(K_J - k) - i\bar{\Gamma}_J} \right), \quad (A10)$$

where $J = P, C$ and γ_J is a coupling constant between a discrete ring mode and the continuous waveguide mode of the actual input channel at the frequency band J. The field enhancement factors for the output channels, $F_{S+}^{(n)}(k)$, are given by

$$F_{S+}^{(n)}(k) = \frac{1}{\sqrt{\mathcal{L}}} \left(\frac{\left(\gamma_S^{(n)}\right)^*}{v_S^{(n)}\left(K_S^{(n)} - k\right) + i\bar{\Gamma}_S} \right), \quad (A11)$$

where now the coupling constant, group velocity, and center wave number depend on the output channel n. The coupling constant for a given channel is related to the intensity decay rate into that channel, as introduced earlier [21]. For simplicity, we assume that the coupling constants are real.

Putting Eqs. (A7)–(A9) into Eq. (10), the nonlinear coefficient for SFWM can be written as

$$K^{nn'}(k_1, k_2, k_3, k_4) = \frac{\hbar^2 \epsilon_0 v_P v_C}{12\pi^2} \bar{\gamma}_{nl} \omega_S \mathcal{L} F_{S+}^{(n)*}(k_1)$$
$$\times F_{S+}^{(n')*}(k_2) F_{P-}(k_3) F_{C-}(k_4), \quad (A12)$$

where we have introduced the nonlinear parameter [21]

$$\bar{\gamma}_{nl} = \frac{3\sqrt{\omega_P \omega_C}}{4\epsilon_0 v_P v_C \mathcal{L}} \int_{\text{ring}} d\boldsymbol{r}_\perp d\zeta \, \Gamma_{(3)}^{ijkl}(\boldsymbol{r})$$
$$\times d_S^{*i}(\boldsymbol{r}_\perp; \zeta) d_S^{*j}(\boldsymbol{r}_\perp; \zeta) d_P^k(\boldsymbol{r}_\perp; \zeta) d_C^l(\boldsymbol{r}_\perp; \zeta) e^{i\Delta\kappa\zeta}, \quad (A13)$$

which has units of $(\text{W m})^{-1}$, and $\Delta k = \kappa_P + \kappa_C - 2\kappa_S$ is the phase-matching function. Now to obtain an effective second-order nonlinear coefficient in the ring, we put Eq. (A12) into Eq. (A5) and find

$$\Lambda^{nn'}(k_1, k_2, k_3, t) = -\frac{\hbar v_P v_C \bar{\gamma}_{NL} \omega_S \mathcal{L}}{4\pi^2} \sqrt{\frac{2\pi P_C}{\hbar \omega_C v_C}}$$
$$\times F_{S+}^{(n)*}(k_1) F_{S+}^{(n')*}(k_2) F_{P-}(k_3)$$
$$\times F_{C-}(K_C) e^{-i\Omega_{nn'}(k_1,k_2,k_3,K_C)t}. \quad (A14)$$

Then putting Eq. (A14) into Eq. (A4), we obtain the nonlinear Hamiltonian for an effective $\chi^{(2)}$ interaction in a ring resonator. In order to work with this Hamiltonian numerically, the wave numbers in all channels have to be discretized. Each waveguide mode has a discrete label j such that its wave

number is given by $k_j = 2\pi m_j/L$, where m_j is an integer mode number and L is the quantization length [10]. Using this discrete notation, the nonlinear Hamiltonian in Eq. (A4) can be written as

$$\bar{H}_{NL}(t) = \hbar \sum_{n,n'} \sum_{i,j,l} \Lambda_{ijl}^{nn'}(t) a_{nSi}^{\dagger} a_{n'Sj}^{\dagger} b_{Pl} + \text{H.c.}, \quad \text{(A15)}$$

where we defined

$$\Lambda_{ijl}^{nn'}(t) \equiv \left(\frac{2\pi}{L}\right)^{3/2} \Lambda^{nn'}(k_{1i}, k_{2j}, k_{3l}, t), \quad \text{(A16)}$$

where $\Lambda^{nn'}(k_{1i}, k_{2j}, k_{3l}, t)$ is the effective second-order nonlinear coefficient for the ring given in Eq. (A13), and the operators satisfy the commutation relations

$$[a_{nJi}, a_{nJj}^{\dagger}] = [b_{Pi}, b_{Pj}^{\dagger}] = \delta_{ij}. \quad \text{(A17)}$$

The Hamiltonian in Eq. (A15) can be written equivalently as

$$\bar{H}_{NL}(t) = \hbar \sum_{(i,n),(j,n')} \sum_{l} \Lambda_{(i,n)(j,n')l}(t)$$
$$\times a_{S(i,n)}^{\dagger} a_{S(j,n')}^{\dagger} b_{Pl} + \text{H.c.} \quad \text{(A18)}$$

We then introduce the discrete indices μ and ν that are constructed by grouping the labels i and n, and j and n' together as

$$\mu \equiv (i, n), \quad \text{(A19)}$$

$$\nu \equiv (j, n'), \quad \text{(A20)}$$

where μ refers to a photon in the output channel n with wave number k_i. With this labeling, we obtain the Hamiltonian in Eq. (32).

APPENDIX B: DERIVING EQUATIONS FOR THE GAUSSIAN PARAMETERS

In this Appendix we show how Eq. (48) for $U_a(t)$ leads to Eqs. (50) and (51) for $V(t)$ and $W(t)$ and how Eq. (49) for $U_b(t)$ leads to Eqs. (52) and (53) for $\beta(t)$ and $\theta_b(t)$.

Beginning with Eq. (48) for $U_a(t)$, it was pointed out earlier [22] that, with an $H_a(t)$ of the form (44), its unique solution can indeed be written as (37). The task here is just to identify how the parameters in $U_a(t)$ depend on time for a specified $H_a(t)$. The strategy that we employ relies on introducing time-dependent output operators $a(t)$ defined as

$$a(t) = U_a^{\dagger}(t) a U_a(t) \qquad = V(t)a + W(t)a^{\dagger}, \quad \text{(B1)}$$

where $V(t)$ and $W(t)$ are found to be given by [22]

$$V(t) \equiv \cosh[u(t)] e^{i\phi(t)}, \quad \text{(B2)}$$

$$W(t) \equiv \sinh[u(t)] e^{i\alpha(t)} e^{-i\phi^{\mathrm{T}}(t)} \quad \text{(B3)}$$

and where the Hermitian matrices $u(t)$ and $\alpha(t)$ that appear here come from the polar decomposition of the squeezing matrix,

$$J(t) = u(t) \exp[i\alpha(t)]. \quad \text{(B4)}$$

The matrices $V(t)$ and $W(t)$ in Eqs. (B2) and (B3) satisfy the constraints

$$V(t)V^{\dagger}(t) - W(t)W^{\dagger}(t) = I, \quad \text{(B5)}$$

$$V(t)W^{\mathrm{T}}(t) - W(t)V^{\mathrm{T}}(t) = 0, \quad \text{(B6)}$$

which are necessary so that the operators in Eq. (B1) satisfy the usual equal time bosonic commutation relations. Taking the time derivative of the first line in Eq. (B1), we obtain the equation of motion

$$\frac{da(t)}{dt} = \frac{i}{\hbar} U_a^{\dagger}(t)[H_a(t), a] U_a(t), \quad \text{(B7)}$$

where we used Eq. (48). Now using Eqs. (44) and (B1), Eq. (B7) becomes

$$\frac{da(t)}{dt} = -2i\zeta(t)W^*(t)a - 2i\zeta(t)V^*(t)a^{\dagger}, \quad \text{(B8)}$$

where $\zeta(t)$ is given by Eq. (54). On the other hand, taking the time derivative of the second line in Eq. (B1), we have equivalently

$$\frac{da(t)}{dt} = \frac{dV(t)}{dt}a + \frac{dW(t)}{dt}a^{\dagger}. \quad \text{(B9)}$$

Since the expressions for $da(t)/dt$ in Eqs. (B9) and (B8) are equivalent, we can equate the elements of the matrix coefficients multiplying the a and $a^{\dagger}$ operators in each expression, leading to the coupled equations (50) and (51).

Next we turn to deriving Eq. (52) for $\beta(t)$ and Eq. (53) for $\theta_b(t)$. We start by multiplying Eq. (49) by $U_b^{\dagger}(t)$ from the left

$$i\hbar U_b^{\dagger}\frac{dU_b(t)}{dt} = \hbar[\gamma(t)]_l b_l^{\dagger} + \text{H.c.}, \quad \text{(B10)}$$

where $\gamma(t)$ is given by Eq. (55). Putting Eq. (38) into the left-hand side of Eq. (B10), we obtain

$$i\hbar D_b^{\dagger}\frac{dD_b(t)}{dt} - \hbar\frac{d\theta_b(t)}{dt} = \hbar[\gamma(t)]_l b_l^{\dagger} + \text{H.c.} \quad \text{(B11)}$$

The derivative of the displacement operator is obtained by disentangling it and using the chain rule. Doing this, we obtain

$$i\hbar D_b^{\dagger}\frac{dD_b(t)}{dt} = i\hbar\frac{d[\beta(t)]_l}{dt}b_l^{\dagger} + \frac{i}{2}\hbar\frac{d[\beta(t)]_l}{dt}[\beta^*(t)]_l + \text{H.c.} \quad \text{(B12)}$$

Putting Eq. (B12) into Eq. (B11) and collecting terms, we obtain

$$0 = \left(i\frac{d[\beta(t)]_l}{dt} - [\gamma(t)]_l\right)b_l^{\dagger} - \left(i\frac{d[\beta^*(t)]_l}{dt} + [\gamma^*(t)]_l\right)b_l$$
$$+ \frac{i}{2}\left(\frac{d[\beta(t)]_l}{dt}[\beta^*(t)]_l - \frac{d[\beta^*(t)]_l}{dt}[\beta(t)]_l\right) - \frac{d\theta_b(t)}{dt}, \quad \text{(B13)}$$

which leads to Eqs. (52) and (53).

APPENDIX C: EXTRACTING $J(t)$ AND $\phi(t)$ FROM $V(t)$ AND $W(t)$

In this Appendix we show how to numerically extract the squeezing matrix $J(t)$ and the rotation matrix $\phi(t)$

from the solutions $V(t)$ and $W(t)$ of the coupled equations (50) and (51).

We begin by doing a numerical polar decomposition of $V(t)$. Note that Eq. (B2) is already in the form of a polar decomposition, where $\cosh[u(t)]$ is a Hermitian positive-semidefinite (PSD) matrix and $e^{i\phi(t)}$ is a unitary matrix. Since the Hermitian PSD matrix in a polar decomposition is always unique, the diagonal elements of $\cosh[u(t)]$, which we identify by the set $\{s_i(t)\}$, will be unique. Further, since the matrices $\cosh[u(t)]$ and $u(t)$ commute they can be diagonalized by the same unitary transformation. The SVD of $\cosh[u(t)]$ can be written as

$$\cosh[u(t)] = F(t)\mathrm{diag}[s_1(t), \ldots]F^\dagger(t), \qquad (C1)$$

where

$$u(t) = F(t)\mathrm{diag}[r_1(t), \ldots]F^\dagger(t), \qquad (C2)$$

with the unitary matrix $F(t)$ the same in both decompositions, and the set $\{r_i(t)\}$ are the diagonal elements of $u(t)$. Since Eqs. (C1) and (C2) are diagonalizations of PSD Hermitian matrices, we have

$$s_i(t) \geqslant 0 \qquad (C3)$$

and

$$r_i(t) \geqslant 0. \qquad (C4)$$

Writing Eq. (C2) as

$$u(t) = F(t)r(t)F^\dagger(t), \qquad (C5)$$

where $r(t)$ is a diagonal matrix, we have

$$\cosh[u(t)] = \cosh[F(t)r(t)F^\dagger(t)]$$
$$= F(t)\cosh[r(t)]F^\dagger(t) \qquad (C6)$$

or

$$\cosh[u(t)] = F(t)\mathrm{diag}[\cosh r_1(t), \ldots]F^\dagger(t). \qquad (C7)$$

Comparing with Eq. (C1), we obtain

$$s_i(t) = \cosh[r_i(t)], \qquad (C8)$$

and so, given Eq. (C4), we have

$$s_i(t) \geqslant 1. \qquad (C9)$$

Since the singular values $s_i(t)$ are never zero, then $\cosh[u(t)]$ is invertible and then so is $V(t)$. Thus, from the numerical polar decomposition of $V(t)$ we obtain a unique Hermitian matrix $\cosh[u(t)]$ and a unique unitary matrix $e^{i\phi(t)}$. Additionally, from Eq. (C8) we can write Eq. (C2) as

$$u(t) = F(t)\mathrm{diag}\{\mathrm{arccosh}[s_1(t)], \ldots\}F^\dagger(t), \qquad (C10)$$

where by arccosh we mean the non-negative arccosh, by virtue of Eq. (C4). In summary, then, from the numerical polar decomposition of $V(t)$ we immediately obtain the unique matrices $e^{i\phi(t)}$ and $\cosh[u(t)]$, from the diagonalization (C1) we determine the unitary matrix $F(t)$ and the $\{s_i(t)\}$, and then from Eq. (C10) we construct $u(t)$.

Using $u(t)$ in Eq. (C10), we can write

$$\sinh[u(t)] = \sinh[F(t)r(t)F^\dagger(t)]$$
$$= F(t)\sinh[r(t)]F^\dagger(t) \qquad (C11)$$

or equivalently

$$\sinh[u(t)] = F(t)\mathrm{diag}\{\sinh[r_1(t)], \ldots\}F^\dagger(t), \qquad (C12)$$

which can be written as

$$\sinh[u(t)] = F(t)\mathrm{diag}\left(\frac{\sinh[r_1(t)]}{r_1(t)}, \ldots\right)$$
$$\times \mathrm{diag}[r_1(t), \ldots]F^\dagger(t) \qquad (C13)$$

or

$$\sinh[u(t)] = K(t)u(t), \qquad (C14)$$

where we have used Eq. (C2) and let

$$K(t) = F(t)\mathrm{diag}\left(\frac{\sinh[r_1(t)]}{r_1(t)}, \ldots\right)F^\dagger(t), \qquad (C15)$$

with

$$K_i(t) = \frac{\sinh[r_i(t)]}{r_i(t)}. \qquad (C16)$$

Forming $K_i(t)$ seems problematic if $r_i(t) = 0$. Of course, in such an instance the natural choice would be to take $K_i(t)$ to be the limit of Eq. (C16) as $r_i(t) \to 0$, which would give $K_i(t) = 1$. However, one could worry about issues of uniqueness. In fact, we show below that if $r_i(t) = 0$ we can take $K_i(t)$ to be any nonzero number, and the final result of the following calculation of $J(t)$ will be the same.

The matrix $K(t)$ is clearly invertible, since we can identify

$$K^{-1}(t) = F(t)\mathrm{diag}\left(\frac{1}{K_1(t)}, \ldots\right)F^\dagger(t), \qquad (C17)$$

and furthermore we can numerically construct $K^{-1}(t)$ since we know $F(t)$ and the $r_i(t)$. From Eq. (C14) we then have

$$K^{-1}(t)\sinh[u(t)] = u(t) \qquad (C18)$$

and from Eq. (B3) we have

$$K^{-1}(t)W(t) = u(t)e^{i\alpha(t)}e^{-i\phi^{\mathrm{T}}(t)} = J(t)e^{-i\phi^{\mathrm{T}}(t)}, \qquad (C19)$$

so

$$J(t) = K^{-1}(t)W(t)e^{i\phi^{\mathrm{T}}(t)}. \qquad (C20)$$

All the quantities on the right-hand side are known and so we can determine $J(t)$.

To investigate what happens to $J(t)$ when some of the eigenvalues $r_i(t)$ are zero, consider

$$K^{-1}(t)W(t) = F(t)\mathrm{diag}\left(\frac{\sinh[r_1(t)]}{K_1(t)}, \ldots\right)$$
$$\times F^\dagger(t)e^{i\alpha(t)}e^{-i\phi^{\mathrm{T}}(t)}, \qquad (C21)$$

where we used Eqs. (C18) and (C12). Now we can see that for any i for which $r_i(t) = 0$ we will have $\sinh[r_i(t)]/K_i(t) = 0$, regardless of which nonzero value $K_i(t)$ is set. So the eigenvalues $r_i(t)$ that are zero do not contribute to the matrix $J(t)$.

At this point we have identified $J(t)$ and $e^{i\phi(t)}$; we still must extract $\phi(t)$. The $\phi(t)$ appearing in $R_a[\phi(t)]$ of (40) is a Hermitian matrix and so can be diagonalized,

$$\phi(t) = M(t)\mathrm{diag}[\chi_1(t), \ldots]M^\dagger(t), \qquad (C22)$$

where $\boldsymbol{M}(t)$ is a unitary matrix. Thus we have

$$
\begin{aligned}
\mathrm{e}^{i\boldsymbol{\phi}(t)} &= \mathrm{e}^{i\boldsymbol{M}(t)\mathrm{diag}[\chi_1(t),\ldots]\boldsymbol{M}^\dagger(t)} \\
&= \boldsymbol{M}(t)\mathrm{e}^{i\mathrm{diag}[\chi_1(t),\ldots]}\boldsymbol{M}^\dagger(t). \quad (\text{C23})
\end{aligned}
$$

Numerically diagonalizing the identified $\mathrm{e}^{i\boldsymbol{\phi}(t)}$ would naturally lead us to identify $\boldsymbol{\phi}(t)$ as given by Eq. (C22). However, although the eigenvalues of $\mathrm{e}^{i\boldsymbol{\phi}(t)}$ are well defined, the values of the phases appearing in those eigenvalues are not. For example, one could write

$$
\begin{aligned}
\mathrm{e}^{i\boldsymbol{\phi}(t)} &= \boldsymbol{M}(t)\mathrm{e}^{i\,\mathrm{diag}[\chi_1(t)+2\pi m_1(t),\ldots]}\boldsymbol{M}^\dagger(t) \\
&= \mathrm{e}^{i\boldsymbol{M}(t)\mathrm{diag}[\chi_1(t)+2\pi m_1(t),\ldots]\boldsymbol{M}^\dagger(t)}, \quad (\text{C24})
\end{aligned}
$$

where $m_1(t)$, etc., are any integers. Instead of Eq. (C22) an equivalent $\boldsymbol{\phi}(t)$ is given by

$$
\boldsymbol{\phi}(t) = \boldsymbol{M}(t)\mathrm{diag}[\chi_1(t) + 2\pi m_1(t), \ldots]\boldsymbol{M}^\dagger(t). \quad (\text{C25})
$$

However, this ambiguity does not affect the Gaussian unitary operators in Eq. (36), because both Eqs. (C22) and (C25) lead to the same effective $R_a[\boldsymbol{\phi}(t)]$.

To see this, note that if we posit Eq. (C25) we have

$$
[\boldsymbol{\phi}(t)]_{kl} = [\boldsymbol{M}(t)]_{kp}[\chi_p(t) + 2\pi m_p(t)][\boldsymbol{M}^\dagger(t)]_{pl}, \quad (\text{C26})
$$

and so

$$
R_a[\boldsymbol{\phi}(t)] = \mathrm{e}^{ia_k^\dagger[\boldsymbol{M}(t)]_{kp}[\chi_p(t)+2\pi m_p(t)][\boldsymbol{M}^\dagger(t)]_{pl}a_l}. \quad (\text{C27})
$$

Now we set

$$
c_p(t) = [\boldsymbol{M}^\dagger(t)]_{pl}a_l = [\boldsymbol{M}^*(t)]_{lp}a_l, \quad (\text{C28})
$$

so

$$
c_q^\dagger(t) = [\boldsymbol{M}(t)]_{jq}a_j^\dagger. \quad (\text{C29})
$$

Thus

$$
[c_p(t), c_q^\dagger(t)] = \delta_{pq}, \quad (\text{C30})
$$

and the new operators $c_p(t)$ and $c_q^\dagger(t)$ satisfy equal time commutation relations. In terms of them, we can write (C27) as

$$
\begin{aligned}
R_a[\boldsymbol{\phi}(t)] &= \mathrm{e}^{ic_p^\dagger(t)[\chi_p(t)+2\pi m_p(t)]c_p(t)} \\
&= \mathrm{e}^{ic_p^\dagger(t)\chi_p(t)c_p(t)}\mathrm{e}^{2\pi i m_p(t)c_p^\dagger(t)c_p(t)}. \quad (\text{C31})
\end{aligned}
$$

As basis kets we can choose the eigenkets $|\{n\}, t\rangle$ of all the number operators $c_q^\dagger(t)c_q(t)$, where

$$
c_q^\dagger(t)c_q(t)|\{n\}, t\rangle = n_q|\{n\}, t\rangle. \quad (\text{C32})
$$

Then

$$
\mathrm{e}^{2\pi i m_p(t)c_p^\dagger(t)c_p(t)}|\{n\}, t\rangle = \mathrm{e}^{2\pi i m_p(t)n_p}|\{n\}, t\rangle = |\{n\}, t\rangle, \quad (\text{C33})
$$

and since any ket $|\varphi(t)\rangle$ can be written as a superposition of the $|\{n\}, t\rangle$, from (C31) and (C33) we have

$$
\begin{aligned}
R_a[\boldsymbol{\phi}(t)]|\varphi(t)\rangle &= \mathrm{e}^{ic_p^\dagger(t)[\chi_p(t)+2\pi m_p(t)]c_p(t)}|\varphi(t)\rangle \\
&= \mathrm{e}^{ic_p^\dagger(t)\chi_p(t)c_p(t)}|\varphi(t)\rangle. \quad (\text{C34})
\end{aligned}
$$

Thus, the result we find for $R_a[\boldsymbol{\phi}(t)]$ will be the same whether we use Eq. (C22) or (C25), that is, any logarithm of $\mathrm{e}^{i\boldsymbol{\phi}(t)}$ can be used to construct $R_a[\boldsymbol{\phi}(t)]$.

APPENDIX D: DETERMINING THE PHASE $\theta_a(t)$

The phase $\theta_a(t)$ appears in the unitary operator $U_a(t)$ in Eq. (37). In this Appendix we determine this phase following the approach of Ma and Rhodes [22]. Recall that $U_a(t)$ is the solution to the Schrödinger equation (48) with the Hamiltonian $H_a(t)$ defined in Eq. (44). Given the form of $H_a(t)$ in Eq. (44), it follows [22] that the phase $\theta_a(t)$ is given by

$$
\theta_a(t) = -\frac{1}{2}\int_{-\infty}^t dt'\mathrm{tr}\{\boldsymbol{\zeta}^*(t')\tanh[\boldsymbol{u}(t')]\mathrm{e}^{i\boldsymbol{\alpha}(t')}\} + \text{c.c.}, \quad (\text{D1})
$$

where $\boldsymbol{\zeta}(t)$ is defined in Eq. (54) and is related to the coefficients in $H_a(t)$; recall Eq. (B4) for the polar decomposition of the squeezing matrix $\boldsymbol{J}(t) = \boldsymbol{u}(t)\exp[i\boldsymbol{\alpha}(t)]$.

The first-order solution that is discussed in Sec. V is valid when the amount of squeezing is small or the nonlinearity is weak. In this Appendix we show that the phase $\theta_a(t)$ in Eq. (D1) is approximately zero in the first-order solution. In this case, because the entries of the squeezing matrix $\boldsymbol{J}(t)$ are small, we replace $\tanh[\boldsymbol{u}(t')]\exp[i\boldsymbol{\alpha}(t')]$ in Eq. (D1) with $\boldsymbol{u}(t')\exp[i\boldsymbol{\alpha}(t')] = \boldsymbol{J}(t')$ [recall Eq. (B4)]. Doing this, we can write Eq. (D1) approximately as

$$
\theta_a(t) \approx -\frac{1}{2}\int_{-\infty}^t dt'\mathrm{tr}[\boldsymbol{\zeta}^*(t')\boldsymbol{J}(t')] + \text{c.c.} \quad (\text{D2})
$$

However, from Eq. (69) we have that $\boldsymbol{J}(t') = -2i\int_{-\infty}^{t'} dt''\boldsymbol{\zeta}(t'')$. Putting this into Eq. (D2), the term inside the trace is $\boldsymbol{\zeta}^*(t')\boldsymbol{\zeta}(t'')$, which is much smaller than unity. Thus $\theta_a(t)$ is approximately zero.

APPENDIX E: A CONSERVED QUANTITY

We define the operator $\hat{Q}$,

$$
\hat{Q} \equiv \tfrac{1}{2}\boldsymbol{a}^{\dagger\mathrm{T}}\boldsymbol{a} + \boldsymbol{b}^{\dagger\mathrm{T}}\boldsymbol{b}, \quad (\text{E1})
$$

which is a conserved quantity with respect to the full Hamiltonian in Eq. (32), that is,

$$
[\hat{Q}, \bar{H}_{NL}(t)] = 0. \quad (\text{E2})
$$

However, $\hat{Q}$ is not a conserved quantity with respect to the effective Hamiltonian in Eq. (46). In this Appendix we show that the average value of $\hat{Q}$ in the Gaussian limit is nonetheless a conserved quantity.

We begin with expectation value of $\hat{Q}$ using the ket in the Gaussian limit given by Eq. (57),

$$
\begin{aligned}
\langle\hat{Q}\rangle &\equiv \langle\bar{\psi}_G(t)|\hat{Q}|\bar{\psi}_G(t)\rangle \\
&= \tfrac{1}{2}\mathrm{tr}[\boldsymbol{W}^\dagger(t)\boldsymbol{W}(t)] + [\boldsymbol{\beta}^*(t)]^\mathrm{T}\boldsymbol{\beta}(t). \quad (\text{E3})
\end{aligned}
$$

In what follows we drop the time dependence of $\boldsymbol{W}(t)$ and $\boldsymbol{\beta}(t)$ for convenience. This quantity is conserved if its time derivative is zero

$$
\frac{d\langle\hat{Q}\rangle}{dt} = 0. \quad (\text{E4})
$$

Putting Eq. (E3) into Eq. (E4), we obtain

$$
\tfrac{1}{2}\mathrm{tr}A + B = 0, \quad (\text{E5})
$$

where we have defined

$$A \equiv \frac{d\boldsymbol{W}^{\dagger}}{dt}\boldsymbol{W} + \boldsymbol{W}^{\dagger}\frac{d\boldsymbol{W}}{dt}, \tag{E6}$$

$$B \equiv \sum_{l}\left(\frac{d\beta_l^*}{dt}\beta_l + \beta_l^*\frac{d\beta_l}{dt}\right). \tag{E7}$$

Now we use the differential equations for β_l and $\boldsymbol{W}$ in Eqs. (52) and (51) to simplify A and B. First, to simplify B we put Eq. (52) into Eq. (E7),

$$
\begin{aligned}
B &= i\sum_{i,k,j}\gamma_{kji}\beta_i[\boldsymbol{V}^*\boldsymbol{W}^{\dagger}]_{kj} - i\sum_{i,k,j}\gamma_{kji}^*\beta_i^*[\boldsymbol{V}\boldsymbol{W}^{\mathrm{T}}]_{kj} \\
&= i\sum_{k,j}[\boldsymbol{\zeta}]_{kj}[\boldsymbol{V}^*\boldsymbol{W}^{\dagger}]_{kj} - i\sum_{k,j}[\boldsymbol{\zeta}^*]_{kj}[\boldsymbol{V}\boldsymbol{W}^{\mathrm{T}}]_{kj} \\
&= i\,\mathrm{tr}(\boldsymbol{\zeta}\boldsymbol{W}^*\boldsymbol{V}^{\dagger}) - i\,\mathrm{tr}(\boldsymbol{\zeta}^*\boldsymbol{W}\boldsymbol{V}^{\mathrm{T}}).
\end{aligned} \tag{E8}
$$

Next we simplify A by putting Eq. (51) into Eq. (E6) and obtain

$$A = 2i\boldsymbol{V}^{\mathrm{T}}\boldsymbol{\zeta}^*\boldsymbol{W} - 2i\boldsymbol{W}^{\dagger}\boldsymbol{\zeta}\boldsymbol{V}^*. \tag{E9}$$

Putting Eqs. (E9) and (E8) into Eq. (E5),

$$
\begin{aligned}
0 &= \tfrac{1}{2}\mathrm{tr}(2i\boldsymbol{V}^{\mathrm{T}}\boldsymbol{\zeta}^*\boldsymbol{W} - 2i\boldsymbol{W}^{\dagger}\boldsymbol{\zeta}\boldsymbol{V}^*) + i\,\mathrm{tr}(\boldsymbol{\zeta}\boldsymbol{W}^*\boldsymbol{V}^{\dagger}) \\
&\quad - i\,\mathrm{tr}(\boldsymbol{\zeta}^*\boldsymbol{W}\boldsymbol{V}^{\mathrm{T}}) \\
&= i\,\mathrm{tr}(\boldsymbol{\zeta}^*\boldsymbol{W}\boldsymbol{V}^{\mathrm{T}}) - i\,\mathrm{tr}(\boldsymbol{\zeta}\boldsymbol{V}^*\boldsymbol{W}^{\dagger}) + i\,\mathrm{tr}(\boldsymbol{\zeta}\boldsymbol{W}^*\boldsymbol{V}^{\dagger}) \\
&\quad - i\,\mathrm{tr}(\boldsymbol{\zeta}^*\boldsymbol{W}\boldsymbol{V}^{\mathrm{T}}),
\end{aligned}
$$

and since $\boldsymbol{W}^*\boldsymbol{V}^{\dagger} = \boldsymbol{V}^*\boldsymbol{W}^{\dagger}$ the right-hand side is zero.

---

[1] R. Schnabel, Squeezed states of light and their applications in laser interferometers, Phys. Rep. **684**, 1 (2017).

[2] C. Weedbrook, S. Pirandola, R. García-Patrón, N. J. Cerf, T. C. Ralph, J. H. Shapiro, and S. Lloyd, Gaussian quantum information, Rev. Mod. Phys. **84**, 621 (2012).

[3] J. Wenger, R. Tualle-Brouri, and P. Grangier, Non-Gaussian statistics from individual pulses of squeezed light, Phys. Rev. Lett. **92**, 153601 (2004).

[4] M. Endo, R. He, T. Sonoyama, K. Takahashi, T. Kashiwazaki, T. Umeki, S. Takasu, K. Hattori, D. Fukuda, K. Fukui, K. Takase, W. Asavanant, P. Marek, R. Filip, and A. Furusawa, Non-Gaussian quantum state generation by multi-photon subtraction at the telecommunication wavelength, Opt. Express **31**, 12865 (2023).

[5] R. E. Slusher, P. Grangier, A. LaPorta, B. Yurke, and M. J. Potasek, Pulsed squeezed light, Phys. Rev. Lett. **59**, 2566 (1987).

[6] Y. Zhao, Y. Okawachi, J. K. Jang, X. Ji, M. Lipson, and A. L. Gaeta, Near-degenerate quadrature-squeezed vacuum generation on a silicon-nitride chip, Phys. Rev. Lett. **124**, 193601 (2020).

[7] Z. Yang, M. Liscidini, and J. E. Sipe, Spontaneous parametric down-conversion in waveguides: A backward Heisenberg picture approach, Phys. Rev. A **77**, 033808 (2008).

[8] S. Blanes, F. Casas, J. Oteo, and J. Ros, The magnus expansion and some of its applications, Phys. Rep. **470**, 151 (2009).

[9] G. Triginer, M. D. Vidrighin, N. Quesada, A. Eckstein, M. Moore, W. S. Kolthammer, J. E. Sipe, and I. A. Walmsley, Understanding high-gain twin-beam sources using cascaded stimulated emission, Phys. Rev. X **10**, 031063 (2020).

[10] N. Quesada, L. G. Helt, M. Menotti, M. Liscidini, and J. E. Sipe, Beyond photon pairs—nonlinear quantum photonics in the high-gain regime: A tutorial, Adv. Opt. Photon. **14**, 291 (2022).

[11] N. Quesada and J. E. Sipe, Effects of time ordering in quantum nonlinear optics, Phys. Rev. A **90**, 063840 (2014).

[12] R. Yanagimoto, E. Ng, A. Yamamura, T. Onodera, L. G. Wright, M. Jankowski, M. M. Fejer, P. L. McMahon, and H. Mabuchi, Onset of non-Gaussian quantum physics in pulsed squeezing with mesoscopic fields, Optica **9**, 379 (2022).

[13] K. Chinni and N. Quesada, Beyond the parametric approximation: Pump depletion, entanglement and squeezing in macroscopic down-conversion, arXiv:2312.09239.

[14] J. Flórez, J. S. Lundeen, and M. V. Chekhova, Pump depletion in parametric down-conversion with low pump energies, Opt. Lett. **45**, 4264 (2020).

[15] S. Ramelow, A. Farsi, Z. Vernon, S. Clemmen, X. Ji, J. E. Sipe, M. Liscidini, M. Lipson, and A. L. Gaeta, Strong nonlinear coupling in a Si$_3$N$_4$ ring resonator, Phys. Rev. Lett. **122**, 153906 (2019).

[16] T. J. Steiner, J. E. Castro, L. Chang, Q. Dang, W. Xie, J. Norman, J. E. Bowers, and G. Moody, Ultrabright entangled-photon-pair generation from an Al Ga As-on-insulator microring resonator, PRX Quantum **2**, 010337 (2021).

[17] V. D. Vaidya, B. Morrison, L. G. Helt, R. Shahrokshahi, D. H. Mahler, M. J. Collins, K. Tan, J. Lavoie, A. Repingon, M. Menotti, N. Quesada, R. C. Pooser, A. E. Lita, T. Gerrits, S. W. Nam, and Z. Vernon, Broadband quadrature-squeezed vacuum and nonclassical photon number correlations from a nanophotonic device, Sci. Adv. **6**, eaba9186 (2020).

[18] Y. Zhang, M. Menotti, K. Tan, V. D. Vaidya, D. H. Mahler, L. G. Helt, L. Zatti, M. Liscidini, B. Morrison, and Z. Vernon, Squeezed light from a nanophotonic molecule, Nat. Commun. **12**, 2233 (2021).

[19] M. Liscidini, L. G. Helt, and J. E. Sipe, Asymptotic fields for a Hamiltonian treatment of nonlinear electromagnetic phenomena, Phys. Rev. A **85**, 013833 (2012).

[20] Z. Vernon, N. Quesada, M. Liscidini, B. Morrison, M. Menotti, K. Tan, and J. E. Sipe, Scalable squeezed-light source for continuous-variable quantum sampling, Phys. Rev. Appl. **12**, 064024 (2019).

[21] M. Banic, L. Zatti, M. Liscidini, and J. E. Sipe, Two strategies for modeling nonlinear optics in lossy integrated photonic structures, Phys. Rev. A **106**, 043707 (2022).

[22] X. Ma and W. Rhodes, Multimode squeeze operators and squeezed states, Phys. Rev. A **41**, 4625 (1990).

[23] M. Houde and N. Quesada, Waveguided sources of consistent, single-temporal-mode squeezed light: The good,

the bad, and the ugly, AVS Quantum Sci. **5**, 011404 (2023).

[24] H. Seifoory, Z. Vernon, D. H. Mahler, M. Menotti, Y. Zhang, and J. E. Sipe, Degenerate squeezing in a dual-pumped integrated microresonator: Parasitic

processes and their suppression, Phys. Rev. A **105**, 033524 (2022).

[25] C. Drago and J. E. Sipe, Deconstructing squeezed light: Schmidt decomposition versus the Whittaker-Shannon interpolation, Phys. Rev. A **110**, 023710 (2024).